Geoderma 195-196 (2013) 23–30

Contents lists available at SciVerse ScienceDirect

Geoderma

journal homepage: www.elsevier.com/locate/geoderma

Effects of organic and inorganic fertilization on soil aggregation in an Ultisol as characterized by synchrotron based X-ray micro-computed tomography

Hu Zhou [a], Xinhua Peng [a,*], Edmund Perfect [b], Tiqiao Xiao [c], Guanyun Peng [c]

[a] State Key Laboratory of Soil and Sustainable Agriculture, Institute of Soil Sciences, Chinese Academy of Sciences, 71 East Beijing Road, Nanjing 210008, PR China
[b] Department of Earth and Planetary Sciences, University of Tennessee, Knoxville, TN 37996-1410, USA
[c] Shanghai Synchrotron Radiation Facility (SSRF), Shanghai Institute of Applied Physics, Chinese Academy of Sciences, Shanghai 201204, PR China

ARTICLE INFO

Article history:
Received 2 February 2012
Received in revised form 18 October 2012
Accepted 11 November 2012
Available online xxxx

Keywords:
Soil aggregation
Computed tomography
Long-term fertilization
Microstructure
Image analysis

ABSTRACT

Long-term fertilization practices generally improve soil aggregation through associated increases in organic matter over time. However, the influence of organic versus inorganic fertilization on aggregate structures may be quite different. In this paper, we aimed to quantify the three-dimensional (3D) microstructure of soil aggregates as influenced by different long-term fertilization practices. Soil aggregates with diameters of approximately 5 mm were collected from an Ultisol with a long-term fertilization trial established in 1986. The treatments were no fertilizer (CK), chemical fertilizer (NPK), and chemical fertilizer plus organic manure (NPK + OM). The aggregate microstructure was determined with synchrotron based X-ray micro-computed tomography (SR-μCT) and digital image analysis techniques. Mean corn yields and soil organic carbon were the highest in NPK + OM, followed by NPK and then by CK. Aggregate stability was highest in NPK + OM, and lowest in NPK. The number of pores, number of pore throats, and number of paths between adjacent nodal pores were all significantly decreased by the NPK + OM treatment relative to the NPK and CK treatments. However, microstructural pore properties were mostly not different between NPK and CK treatments. This study demonstrates that organic fertilization can improve soil aggregation, while inorganic fertilization is ineffective, even after 25 years. The different mechanisms by which organic and inorganic fertilization practices influence soil aggregation deserve further investigation.

1. Introduction

Fertilization has long been an important agronomic practice to enhance soil quality and productivity. Since the 1980s, chemical fertilizers have been widely used in the red soil region, which covers 2.04 million km^2 of the tropical and subtropical area of South China (Huang et al., 2010). Long-term fertilization can enhance soil organic matter (SOM) content, nutrient content as well as produce high crop yields in this region (Hou et al., 2011; Wang et al., 2010; Zhang et al., 2009). However, the effects of fertilization on soil structure in the red soil region are still unclear and both positive and negative effects have been reported. For example, Wang and Yang (2003) found improvement of soil structure with organic manure but no improvement with chemical fertilizer. Lai et al. (1992) reported long-term application of chemical fertilizer increased bulk density and deteriorated soil structure. Studies of soil structure are usually conducted on bulk soil scales and mostly use bulk density, porosity, or stability to describe soil structure. Knowledge of detailed aggregate geometry, however, is very limited. To better understand the fertilization effects on soil aggregation processes it is advantageous to conduct research at the aggregate scale and to investigate aggregate internal geometry directly (Kravchenko et al., 2011; Young et al., 2001). We hypothesized that organic and inorganic fertilization may play different roles in soil aggregation and structure.

Soil aggregation is widely regarded as a key indicator of soil quality that determines water, gas and nutrient retention and transport in soils, and offers numerous micro-habitats for microbial communities (Feeney et al., 2006; Pagliai et al., 2004; Six et al., 2004). Soil aggregation processes, and factors which influence them, have been well documented (Bronick and Lal, 2005; Oades, 1984; Oades and Waters, 1991; Six et al., 2004; Tisdall and Oades, 1982). The red soil is high in metal oxides and clay content and low in organic matter content (Zhang and Horn, 2001). Key aggregation processes have been frequently studied but are still unclear (Huang et al., 2010; Zhang and Horn, 2001; Zhang and Peng, 2006). A detailed study of the internal microstructure of aggregates can provide information regarding soil aggregation processes and thus soil quality.

The traditional method used to visualize and quantify soil structure is to analyze digital images of soil thin sections (Pagliai et al., 2004) or soil blocks (Vogel, 1997; Vogel et al., 1993). Using the thin section approach, Pagliai et al. (1983, 1984, 2004), VandenBygaart et al. (1999), and Drees et al. (1994) studied soil aggregation under different tillage or fertilization treatments. The drawbacks of this method are labor and time costs, destructive sample preparation techniques, and

* Corresponding author. Tel.: +86 25 86881198; fax: +86 25 86881000.
E-mail address: xhpeng@issas.ac.cn (X. Peng).

0016-7061/$ – see front matter © 2012 Elsevier B.V. All rights reserved.
http://dx.doi.org/10.1016/j.geoderma.2012.11.003

its restriction to two-dimensional (2D) images. In recent years a variety of computed tomography (CT) techniques have been introduced and used to non-destructively and quickly explore soil structure in 3D (Young et al., 2001). Luo and Lin (2009), Luo et al. (2008, 2010) studied relationships between soil macropores and preferential flow and transport at the column scale. Udawatta et al. (2006, 2008a, 2008b) determined the influence of grass buffers and agroforestry practices on soil macropore characteristics at different scales. Compared to the widely used medical CT and industrial CT, synchrotron based X-ray micro-CT (SR-μCT) has higher resolution, stronger contrast, and faster scanning speed, and is therefore an excellent tool for studying microstructure of soil aggregate (~1–10 mm in diameter) (Peth et al., 2008; Wildenschild et al., 2002). For example, Peth et al. (2008) analyzed the pore structure of soil aggregates from conventionally-tilled and grassland plots with SR-μCT, and found marked differences in microstructure characteristics between the two aggregates investigated. To date, however, few studies have specifically investigated long-term fertilization effects on 3D aggregate microstructure using SR-μCT.

The hypothesis of this research is that different fertilization practices may lead to different soil aggregation processes leading to observable differences in the morphology and microstructure of soil aggregates. The objective of this study was to quantify the 3D aggregate microstructure with high resolution SR-μCT and digital image analysis methods and to evaluate the effects of different long-term organic and inorganic fertilization practices on soil aggregation.

2. Materials and methods

2.1. Site description and sampling

The long-term fertilization experiment was established on a Red Soil (Genetic Soil Classification of China, corresponding to Ultisols in the Soil Taxonomy System of United States) in 1986 at the Jiangxi Institute of Red Soil (116°26′ E, 28°37′ N), Jinxian City, Jiangxi Province, China. This region has a subtropical climate. Long-term mean annual temperature and precipitation are 17.7 °C and 1727 mm, respectively. The soil has 34.0% clay (<2 μm), 52.7% silt (2–200 μm), and 13.3% sand (200–2000 μm) at the depth 0–20 cm.

The cropping system was continuous corn (spring corn–autumn corn) production. Moldboard plow tillage was implemented to about 20 cm depth before and after the autumn corn season. Manual hoeing was used to prepare the seedbed. Three fertilization treatments were studied: (1) control, no fertilizer was used (CK); (2) inorganic fertilizers applied at the rates of 60 kg N ha^{-1}, 13 kg P ha^{-1}, and 33 kg K ha^{-1} for each corn growing season (NPK); and (3) addition of 15 Mg ha^{-1} (fresh weight) organic pig manure (OM) to the inorganic fertilizers (same rate as NPK) (NPK + OM). The experimental design was a randomized complete block with three replicates in micro-plots of 22.2 m^2.

Soil samples were taken from the top layer (0–15 cm) with a shovel in June 2010. They were partially air-dried at room temperature to about the plastic limit and then divided into two portions. One part, used for tomography scanning, was separated into aggregates by hand along natural failure surfaces. Due to limited synchrotron beam time, five representative aggregates, with diameters of approximately 5 mm, were selected from each treatment for the μ-CT study. The selected aggregates were oven-dried at 40 °C for 24 h and stored at 4 °C before CT scanning. Aggregates of similar size (3–5 mm in diameter) were also collected for the measurement of aggregate stability using the Le Bissonnais' method (1996) with the pretreatment of fast wetting.

The unfractionated sample was ground to pass a 2 mm sieve for measuring some basic soil properties. Soil properties were determined using routine methods (Soil Survey Laboratory Methods Manual, 2004). Soil particle size distribution was measured by the pipette method. Soil organic carbon (SOC) was determined using the method of oxidation with potassium dichromate in a heated oil bath, total nitrogen using the semi micro Kjeldahl method. Total P was digested with perchloric acid and sulfuric acid and determined using colorimetry. Total potassium was determined by means of flame photometry after digestion with hydrofluoric acid and perchloric acid. Soil pH was measured using a glass electrode with a 1:2.5 soil:water ratio. Cation exchange capacity (CEC) was measured by the ammonium acetate method. Corn grain yield was determined by harvesting all the ears within each plot. Grain was removed from the ears and weighed. Corn yield was adjusted to a moisture content of 155 g kg^{-1}.

2.2. CT scanning and image processing

The experiments were carried out at beam line BL13W1 of the Shanghai Synchrotron Radiation Facility (SSRF). Samples were scanned with the SR-μCT at a photon energy of 28 keV. Aggregates were held in a plastic tube which was mounted on a rotary stage. The sample was rotated from 0° to 180° with n (n = aggregate width (μm) × $\frac{\pi}{2}$) absorption radiographs acquired from different angles at the same interval. The filtered back-projection algorithm was used to reconstruct the images. A total of 430 slices, with the size 1052 × 1052 pixels, were reconstructed for each aggregate. The resulting voxel size was 9 × 9 × 9 μm^3, with voxel values ranging from 0 to 255 corresponding to the attenuation coefficient.

As obvious ring artifacts were observed in some images (Fig. 1a), they must be removed before image segmentation. The image was first transformed from Cartesian space into polar space with the Polar transformer plugin (Donnelly and Mothe, 2008) in ImageJ (Rasband, 2010). The periodic ring artifacts were realized as straight lines in the frequency domain and removed by masking the Fourier transformed image with a Matlab (The MathWorks Inc., Natick, MA) program.[1] The resulting image was inverse Fourier transformed and then transformed back into Cartesian space. Example images before and after removal of the ring artifact are shown in Fig. 1.

Image segmentation and pore morphology analysis were completed with the 3DMA software (Lindquist and Venkatarangan, 1999). Because 3DMA can only process regularly shaped objects, sub-volumes of size 300 × 360 × 360 voxels (i.e. 2.70 × 3.24 × 3.24 mm^3) were extracted from the central part of each image for further analysis. To minimize the light variation among images of the same sample, stack images were normalized using ImageJ software before batch processing of image segmentation. In this study, we used a locally adaptive segmentation method, i.e. the indicator kriging method (Oh and Lindquist, 1999) to separate soil pores from the solid phase. Briefly, a lower (T_0) and an upper (T_1) limit were selected by visual inspection of the image histograms. Voxel values below T_0 and above T_1 were identified as the pore and solid phases, respectively. Voxels with grayscale values between T_0 and T_1 were classified as pores or solids depending on the local covariance determination. Details of the indicator kriging method are given in the papers of Oh and Lindquist (1999) and Peth et al. (2008).

2.3. Quantification of 3D microstructure

The workflow to analyze the pore space geometry using 3DMA is outlined in Fig. 2. Detailed theories of the processes employed are described in Lindquist and Venkatarangan (1999) and references therein. Firstly, skeletons or medial axes of the pore phase, representing the topological structure of the pore phase, were computed using morphological erosion based on the LKC algorithm (Lee, et al., 1994). The distance between the skeleton and the nearest solid phase was recorded as the burn number. Because the computation of skeletons is sensitive to isolated clusters and irregular boundaries, medial axis trimming must be performed to remove dead end and isolated paths. Isolated

[1] The program is available from the corresponding author.

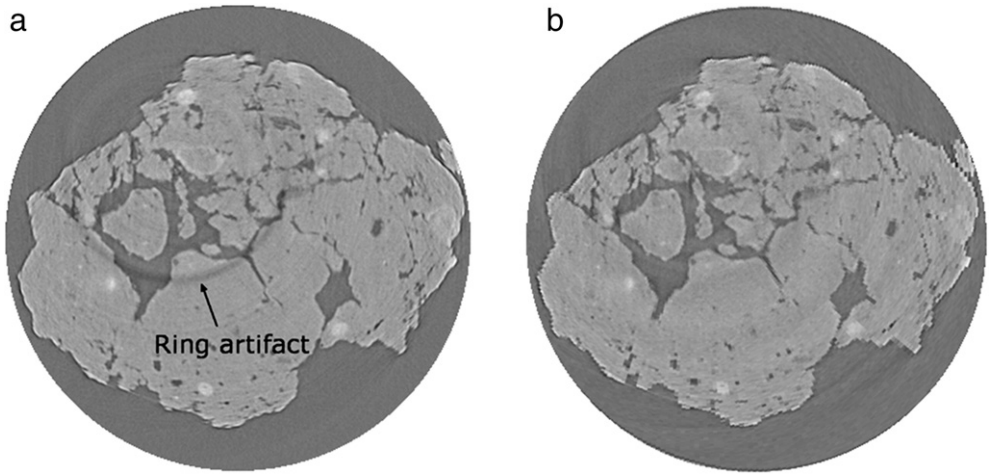

Fig. 1. Reconstructed slice before (a) and after (b) ring artifact correction.

voxels with a burn number less than 2, and branch–leaf paths and needle-eye paths with burn numbers less than the maximum burn number were removed (Peth et al., 2008). The next procedure is to find the pore throats, defined as the minimum cross-sectional area of each channel. Contrary to using erosion to find the medial axes, the pore throats are found by dilating the medial axis to cylinders in the perpendicular direction (Lindquist et al., 2000). The cylinders grow during the dilation process and eventually hit the pore–solid interface. At the contact point the dilation is stopped, while dilation continues at other locations. Finally the perimeters of the throats were found and the throat areas were computed. With throats constructed, pore space was partitioned into nodal pores separated by throat surfaces and the solid phase.

Once the pore–throat-network was constructed, the pore system could be analyzed quantitatively. Measures of the pore system include porosity, nodal pore-size distribution (PSD), pore throat size distribution (TSD), effective throat/pore radii ratio, path length distribution, and tortuosity. The sizes of pores and throats are expressed as equivalent diameters and tortuosity is calculated as the ratio between the path length and the straight distance between the ends of the path. Pores were classified into macropores (>500 μm) and mesopores (≤500 μm) according to their equivalent diameters.

2.4. Statistical analysis

To compare differences in pore system measures among the treatments, analysis of variance (ANOVA) was conducted using the GLM procedure in the SAS software program (SAS institute, 1990). Mean values were tested using the least significant difference method (Duncan's LSD) at the $p = 0.05$ level of statistical significance.

3. Results

3.1. Basic soil properties and crop yields

As listed in Table 1, after 25-year fertilization, SOC, total P, total K, CEC and pH were significantly higher in NPK + OM treatment than in NPK and CK treatments ($P<0.05$), while in the latter two treatments only SOC and total K were statistically different ($P<0.05$). Aggregate stability, as indicated by the mean weight diameter (MWD), was highest in NPK + OM treatment and lowest in the NPK treatment ($P<0.05$). The 25-year mean annual corn yield increased in the order of CK (1683 kg ha^{-1}) < NPK (6960 kg ha^{-1}) < NPK + OM (9948 kg ha^{-1}), while the coefficient of variation (CV) for 25 years' yields decreased in the opposite order: CK (48%) > NPK (27%) > NPK + OM (25%).

3.2. Visualization of soil aggregates

The scanned aggregates (referred to hereafter as macro-aggregates) were composed of smaller aggregates (referred to hereafter as sub-aggregates) as shown in the 2D images (Fig. 3a). The size of the sub-aggregates ranged from 1.5 to 2 mm for the NPK + OM treatment while mostly <1 mm for the NPK and CK treatments. Pores within the macro-aggregates were visually classified as inter- or intra-sub-aggregate pores based on their position relative to the sub-aggregates. Inter-sub-aggregate pores from the NPK + OM treatment included channels and vughs, while those from the NPK and CK treatments were dominated by vughs (Fig. 3a). The NPK + OM treatment had fewer numbers of inter-sub-aggregate pores than either the NPK or CK treatments. While more intra-sub-aggregates pores were observed in the NPK + OM treatment, suggesting a more porous sub-aggregate

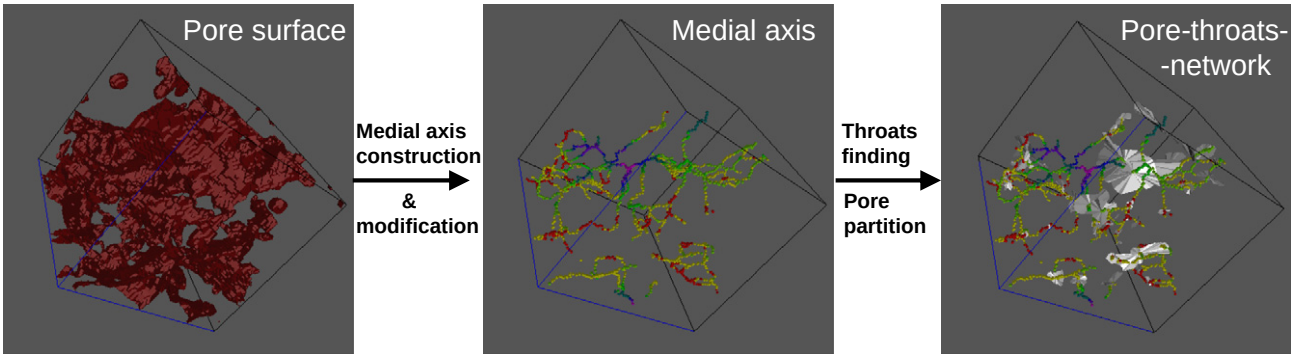

Fig. 2. Schematic sequential diagram of the pore–throat network construction.

Table 1
Basic soil properties and crop yield as affected by long-term fertilization.

Treatments	SOC* (g kg^{-1})	Total N (g kg^{-1})	Total P (g kg^{-1})	Total K (g kg^{-1})	pH (H_2O)	CEC (cmol kg^{-1})	MWD (mm)	Corn yield (kg ha^{-1})	CV of 25 years' yield (%)
CK	7.98 (0.39)†c‡	1.03 (0.26)a	0.56 (0.04)b	12.98 (0.20)b	3.98 (0.07)b	10.77 (0.40)b	0.64 (0.01)b	1683 (30)c	48
NPK	9.87 (0.50)b	1.04 (0.13)a	0.68 (0.10)b	13.53 (0.38)a	3.90 (0.07)b	11.53 (0.23)b	0.45 (0.08)c	6960 (151)b	27
NPK + OM	12.10 (0.91)a	1.17 (0.24)a	1.59 (0.08)a	13.56 (0.22)a	4.83 (0.07)a	13.97 (0.47)a	0.77 (0.11)a	9948 (247)a	25

* SOC, soil organic carbon; CEC, cation exchange capacity; MWD, mean weight diameter; CV, coefficient of variation.
† Values in parentheses represent the standard deviation of the mean.
‡ Different letters following values between different fertilization treatments indicate significant difference at the P<0.05 level (LSD).

structure as compared to the NPK and CK treatments. An overall perspective of the pore structure can be inferred from the 3D images of the pore systems (Fig. 3b). The pore systems for the NPK and CK treatments were less continuous than those of the NPK + OM treatment.

3.3. Quantification of pore–throat-networks

3.3.1. Porosity and pore-size distribution

The pores discussed here excluded the smallest pores that could not be resolved due to resolution limitations. General statistical information about the pores and pore throat networks within individual aggregates from the different tillage treatments is given in Table 2. The total porosity showed no statistically significant (P > 0.05) difference among the CK, NPK, and NPK + OM treatments. However, if total pores were separated into macro- and mesopores, the macroporosity for the NPK + OM treatment was significantly higher than for the CK and NPK treatments (P < 0.05). Pores connected to, or not connected to, the outside of the analyzed volume were named boundary and interior pores, respectively. The numbers of interior and boundary pores as well as the total number of pores for the NPK + OM treatment were all less than for the NPK treatment, and significantly less than for the CK treatment (P < 0.05), but there was no difference between NPK and CK treatments. The fractions of interior and boundary pores for the NPK and NPK + OM treatments were not significantly different, but both were significantly different (lower and higher, respectively) from the CK treatment (P < 0.05).

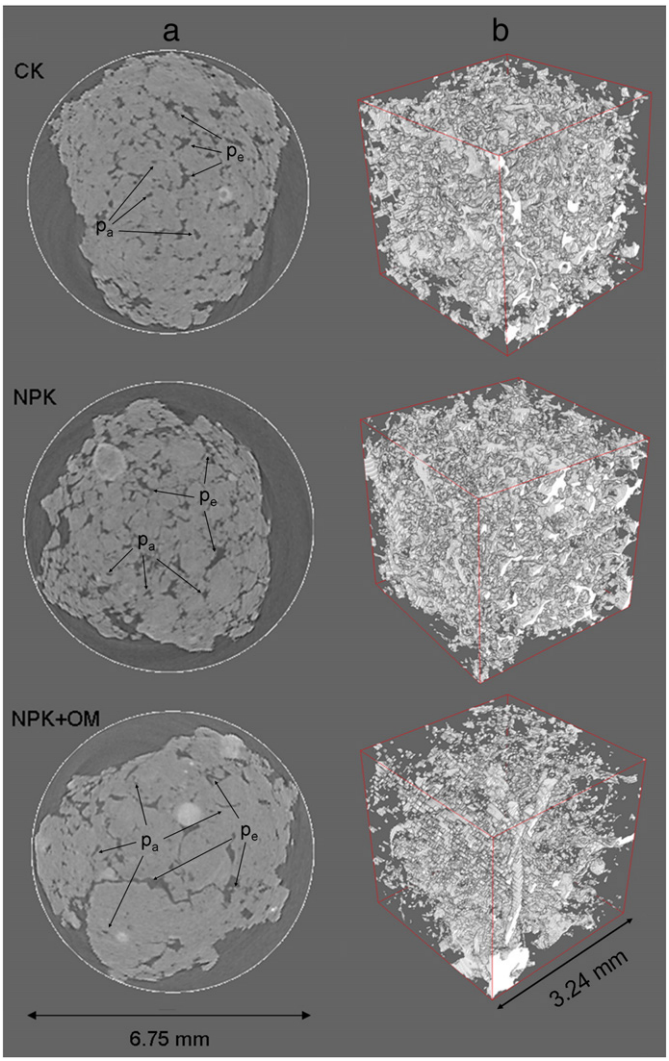

Fig. 3. Representative 2D and 3D visualizations of soil aggregate structures from the different fertilization treatments: NPK + OM, chemical fertilizer and organic manure; NPK, chemical fertilizer; CK, no fertilizer. p_e, inter-sub-aggregate pores; p_a, intra-sub-aggregate pores.

The nodal pore size distribution showed clear evidence of bimodal patterns, with pores larger than 500 μm sparsely distributed on the right hand side of the graph (Fig. 4). The NPK + OM treatment had the lowest porosity within the 10–500 μm range due to less inter-sub-aggregate pores. The porosities for the pores with an effective diameter larger than 500 μm differed in the order: NPK + OM > NPK > CK, which was consistent with the macroporosity. In general, the pore size distribution under NPK + OM was much different from those for the NPK and CK aggregates, but the latter two were close.

3.3.2. Path length

Path length refers to the distance between the centers of any two adjacent nodal pores. This distance is measured along the medial axis rather than along the straight line between the two centers. The number–size distribution of paths exhibited a log-normal distribution as shown in Fig. 5. The path lengths ranged from 9 to 2079, 9 to 1422, and 9 to 1575 μm for the NPK + OM, NPK, and CK treatments, respectively (Fig. 5). Marked differences in path lengths were observed among the treatments. The number of paths in the NPK + OM treatment

Table 2
Summary of soil aggregate microstructure properties from three long-term fertilization treatments.

Pore properties	CK	NPK	NPK + OM
Porosity (%)	14.2 (1.7)*a†	14.9 (2.3)a	13.2 (1.3)a
Macroporosity (>500 μm) (%)	3.4 (0.6)b	3.6 (0.7)b	6.7 (0.4)a
Mesoporosity (≤500 μm) (%)	10.8 (1.1)a	11.3 (1.6)a	6.5 (0.9)b
Total no. of pores	3308 (313)a	2695 (267)ab	2288 (502)b
No. of interior pores	2676 (407)a	2189 (268)ab	1881 (352)b
No. of boundary pores	632 (250)a	505 (87)ab	404 (68)b
Fraction interior pores (%)	55.2 (5.2)a	29.3 (2.9)b	33.0 (7.2)b
Fraction boundary pores (%)	44.8 (5.2)b	70.7 (2.9)a	67.0 (7.2)a
Total no. of throats	3709 (704)a	2698 (432)ab	1526 (257)b
Mean area of throats (μm^2)	2913 (337)a	3803 (469)a	3148 (342)a
Specific surface area (mm^{-1})	8.50 (1.50)a	7.80 (1.81)a	5.80 (2.62)a
Total no. of paths	6218 (1028)a	4937 (1346)a	3277 (988)b
Average length of paths (μm)	158 (14)a	169 (27)a	175 (19)a
Average tortuosity of paths	1.96 (0.34)a	2.03 (0.28)a	2.05 (0.19)a

* Values in parentheses represent the standard deviation of the mean.
† Different letters following values between different fertilization treatments indicate significant difference at the P<0.05 level (LSD).

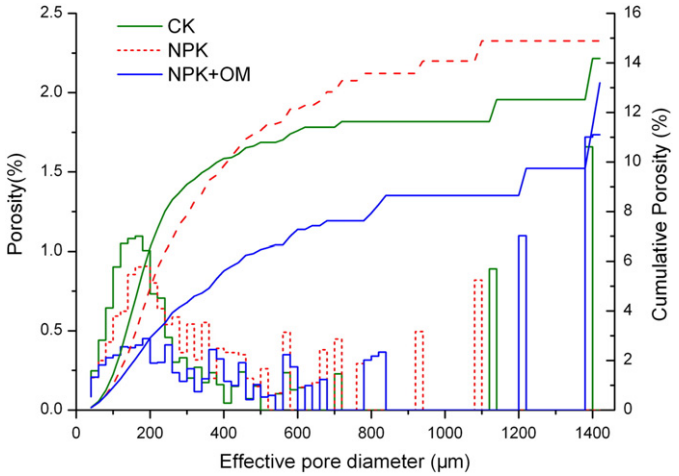

Fig. 4. Pore-size distributions for soil aggregates from the different fertilization treatments: NPK + OM, chemical fertilizer and organic manure; NPK, chemical fertilizer; CK, no fertilizer.

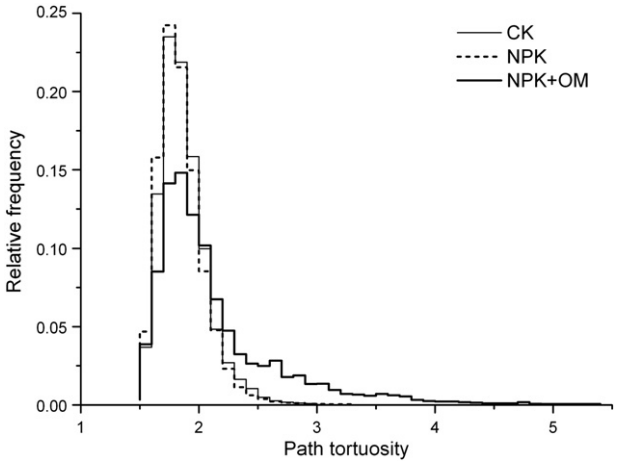

Fig. 6. Pore tortuosity as a function of direction for a representative aggregate (a) and average tortuosity values (b) for soil aggregates from the different fertilization treatments: NPK + OM, chemical fertilizer and organic manure; NPK, chemical fertilizer; CK, no fertilizer.

was significantly lower than in the NPK and CK treatments ($P<0.05$) for the 50–500 μm region, while no significant difference ($P>0.05$) was found between the latter two treatments.

The number of paths with lengths of >500 μm was relatively small and no significant differences were observed between the treatments. However, the NPK + OM treatment had the longest right hand side tail among the treatments (Fig. 5), and the existence of longer pores in this treatment was also evident in Fig. 3.

3.3.3. Path tortuosity

The relative frequency of path tortuosity increased with increasing tortuosity up to ~1.8 and then declined with increasing tortuosity (Fig. 6). The relative frequencies in the NPK + OM treatment were lower than in the NPK and CT treatments for tortuosity of <2 and higher for tortuosity of >2. Little difference in tortuosity was found between the CT and NPK treatments. The maximum tortuosity values were 5.4, 3.3, and 3.1 for NPK + OM, NPK, and CT treatments, respectively. The most irregular paths, with tortuosity values larger than 3.3, were only observed in the NPK + OM treatment.

3.3.4. Pore throats

In addition to pore size and path tortuosity, fluid flow within the pore system is greatly influenced by the bottlenecks (throats) of the interconnected pores. Throats of the pore system were extracted to separate the interconnected pores, and their surface areas were computed. A log-normal distribution of the pore throat surface areas was observed (Fig. 7). The total number of pore throats for the NPK + OM treatment was significantly lower than for the NPK and CT treatments (Table 2). The pore throat area distributions showed the same trend, except for the largest pore throats (Fig. 7a). The NPK + OM treatment had the largest pore throat surface area (0.22 mm^2), compared to 0.11, and 0.06 mm^2 for the NPK and CT treatments, respectively.

The effective throat/pore radius ratio ranged from 0.05 to 1.00, 0.05–1.05, and 0.05–1.25 for the NPK + OM, NPK, and CK treatments, respectively (Fig. 7b). The number of throat/pore pairs increased sharply with increasing effective throat/pore radius ratio up to ~0.15 and then declined with increasing effective throat/pore radius ratio (Fig. 5). Similar to the pore throat area distribution, the number distribution of pore throat/pore radius ratios increased in the order: CT > NPK > NPK + OM (Fig. 5), especially within the 0.05–0.5 range (Fig. 7b).

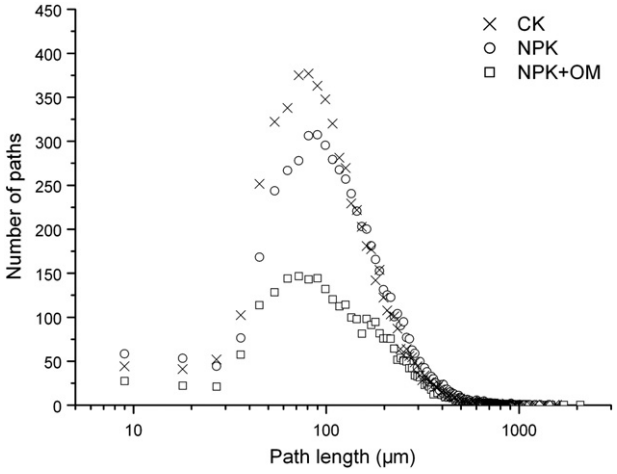

Fig. 5. Path length distribution for soil aggregates from the different fertilization treatments: NPK + OM, chemical fertilizer and organic manure; NPK, chemical fertilizer; CK, no fertilizer.

4. Discussion

4.1. Effects of fertilization on soil aggregation

Organic and inorganic fertilizers have complex effects on soil physical, chemical and biological properties, resulting in variable effects on soil aggregation (Bronick and Lal, 2005). Generally, application of organic manure directly increases soil organic matter (SOM), leading to improved soil aggregation and enhanced stability. These trends are usually indicated by increases in macro-aggregate content and the mean weight diameter (MWD) of water-stable aggregates, as well as by decreases in bulk density (Bronick and Lal, 2005; Haynes and Naidu, 1998; Sainju et al., 2003; Whalen and Chang, 2002). In this study, long-term fertilization, particularly the application of NPK + OM, not only increased SOC, aggregate stability, and other soil nutrients but also improved crop yield with reduced variability (Table 1). At the same experimental site, Huang et al. (2010) observed significantly more macro-aggregates and higher SOM content in the bulk soil and the >2 mm aggregate fraction for the NPK + OM treatment than in the other treatments. The enrichment of SOC, either from crop residues or from direct-applied organic manure, has been documented to improve soil aggregation (Six et al., 1998, 2004). However, in this study the chemical fertilizer alone (NPK) showed an inverse effect on aggregate stability as compared with the no fertilization treatment (CK), although it contained more SOC content (Table 1). This is consistent

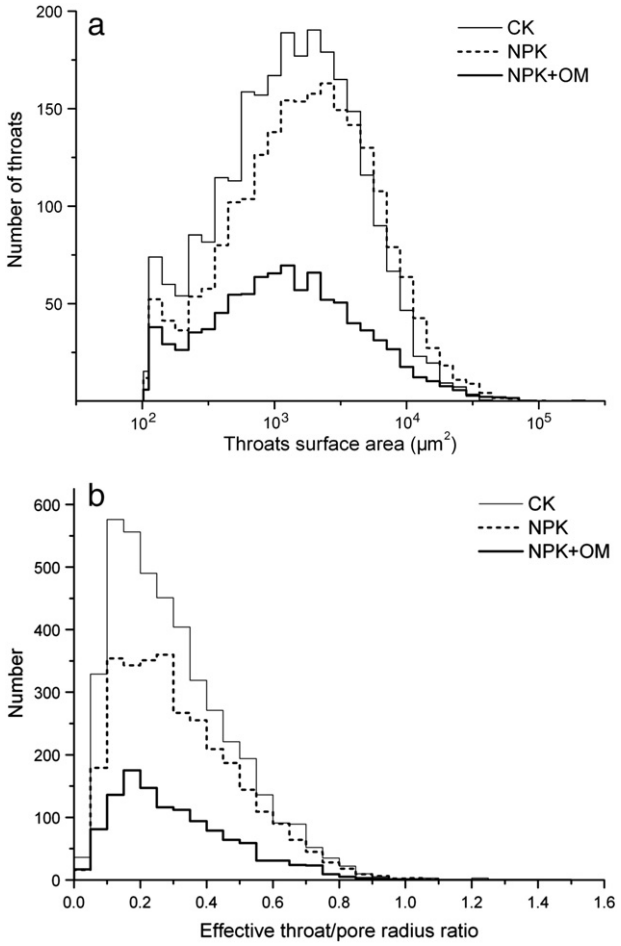

Fig. 7. Pore throat surface area (a) and effective throat/pore radius ratio distribution (b) for soil aggregates from the different fertilization treatments: NPK + OM, chemical fertilizer and organic manure; NPK, chemical fertilizer; CK, no fertilizer.

with Lai et al. (1992) who reported that application of only chemical fertilizer degraded soil structure in the studied region. We have demonstrated differences in micro-aggregate structures associated with long-term chemical versus organic fertilization. Elucidation of the underlying mechanisms responsible for these different structures will need further work.

4.2. Relation between soil aggregation and microstructure

The scanning images indicated that the macro-aggregates were formed by a group of sub-aggregates, which were a combination of smaller aggregates or particles, showing a hierarchical structure (Fig. 3). The NPK + OM treatment had fewer numbers of inter-sub-aggregate pores than either the NPK or CK treatments. This trend was ascribed to the greater development and coalescence of smaller sub-aggregates in the NPK + OM treatment. The 3D pore systems for the CK and NPK treatments exhibited similar honeycomb patterns, while more continuous longer channels were only found in the NPK + OM treatment.

The pore morphological parameters, including porosity, pore-size distribution, pore throat area, path length, and tortuosity, quantitatively illustrated the main structural differences between aggregates from the different treatments. The NPK + OM treatment had the highest macroporosity and the lowest mesoporosity (Table 2). The higher macroporosity indicates easier transport of water and nutrients in the NPK–OM treatment. Path number was lower in the NPK + OM treatment as compared to in the NPK and CK treatments, however, the NPK + OM treatment had the longest paths (Fig. 5). The existence of longer pores under NPK + OM was also evident in Fig. 3. The continuous longest paths formed by roots or soil fauna can have a major effect on soil water flow (Peth et al., 2008). Application of organic manure (e.g., NPK + OM) significantly decreased the number of pore throats and increased their throats surface area. Consequently, it decreased the ratio of pore throat/pore radius ratios (Fig. 7). This also suggests that organic fertilization will improve water, gas and nutrient fluxes as compared to inorganic fertilization. On the other hand, application of NPK + OM further improved soil aggregation and decreased the number of pore throats while increasing the throat surface area. These quantitative results, together with the 2D and 3D observations, indicated that aggregates from the NPK + OM treatment were more developed and their sub-aggregates were more organized as compared to the CK and NPK treatments. From aggregate microstructure, the application of chemical fertilizer (NPK) alone, however, showed no significant improvement of soil aggregation, which is consistent with aggregate stability. These results support our hypothesis that enhanced SOM from organic fertilization promotes soil aggregation and alters the microstructure, and clearly indicate the different effects of organic and inorganic fertilizers on soil aggregation.

4.3. Quantification of aggregate structure in 3D

With the rapid development of tomography techniques, high resolution tomography facilities are becoming more available, permitting direct study of the internal microstructure of soil aggregates. The challenge now is image processing and analysis, of which one critical step is image segmentation (Baveye et al., 2010; Iassonov et al., 2009; Schlüter et al., 2010; Wang et al., 2011). Although numerous segmentation methods, including global thresholding and local adaptive segmentation method, have been proposed, none is widely accepted in the study of the CT images of soil (Iassonov et al., 2009). In this study, we used a locally adaptive segmentation method, i.e. the indicator kriging method (Oh and Lindquist, 1999). The indicator kriging method was tested by Iassonov et al. (2009) and Wang et al. (2011) and proved to yield promising results. It has been successfully used in several soil studies (e.g. Kravchenko et al., 2011; Peth et al., 2008; Udawatta et al., 2008b). However, this method is subjective on choosing the T_0 and T_1 values, which makes results from different studies hard to compare. This limitation may be overcome by the developing advanced local adaptive method. Meanwhile, the capability to acquire high resolution, high contrast and low noise images will help to properly segment the tomography image.

The second step is to find suitable measures to quantify the complex soil structure (Schlüter et al., 2011). Pore-size distribution, which is expressed in terms of the frequency distribution of logarithmic effective radii, is one of the most important parameters. In this study, we quantified the detailed aggregate microstructure not only for the pore-size distribution but also for key shape parameters (i.e. throat area, path length, and path tortuosity). Our results showed that these parameters are also capable of differentiating between fertilization treatments in terms of aggregate microstructure.

Shape parameters have been used to characterize soil structure in previous studies (Lindquist and Venkatarangan, 1999; Peth et al., 2008; Udawatta et al., 2008b). However, due to vastly different study scales and resolutions of the tomography images, results from different studies are hard to compare. For example, the tortuosity values measured in this study are larger than those reported by Perret et al. (1999) (1.12–1.17), Jassogne et al. (2007) (1.5–2.5) and Luo et al. (2010) (1.32–1.82), who focused mainly on soil macropores formed by soil fauna or plant roots. We focused on inter-aggregate pores and the high resolution capability revealed the complex micro- and mesopores that were more irregular (Peth et al., 2008; Udawatta et al., 2008b). Another example is the path length; the maximum path length ranged from 0.6 mm in study of Peth et al. (2008), to 2 mm in the present study, to 40 mm in Perret et al. (1999). Therefore, the

contribution of the longest path to soil water movement needs to be evaluated carefully because of the different scales of interest.

With high resolution tomography and image analysis, the measurement of aggregate microstructure can provide very detailed characterization of soil aggregation, which was usually overlooked in the past. In the near future, it is likely that computed tomography will become increasingly popular as a powerful tool for investigating soil aggregation.

5. Conclusions

This study investigated the three dimensional microstructural characteristics of soil aggregates from NPK + OM, NPK, and CK fertilization treatments using SR-μCT and digital image analysis techniques. We found that application of NPK + OM increased the size of sub-aggregates that comprised the macro-aggregates. The mesoporosity, number of pores, number of pore throats, and number of paths all decreased in the NPK + OM treatment relative to the other treatments. The macroporosity, mean area of throats, and average path length increased in the NPK + OM treatment compared to the CK treatment. Relatively small differences in pore morphology parameters were found between NPK and CK treatments. Our results indicate that long-term application of NPK + OM improves soil aggregation and alters the three-dimensional microstructure of macro-aggregates, while NPK alone does not. This confirms our hypothesis that fertilization is able to change soil microstructure but this process depends upon the fertilization practice. Our future studies will explore the nature of different binding agents and the effects of different microstructures on nutrient retention at the aggregate scale.

Acknowledgments

This work was supported by National Natural Science Foundation of China (nos. 41101200 and 41171180), Innovation Program of Institute of Soil Science, CAS (ISSASIP1111), and the "100 Talents Program" of The Chinese Academy of Sciences. The authors thank SSRF (Shanghai Synchrotron Radiation Facility) for supporting the use of the radiation source. We also thank Mr. Yu Xichu, Institute of Red Soil, Jiangxi province, for providing the soil samples.

References

Baveye, P.C., Laba, M., Otten, W., Bouckaert, L., Sterpaio, P.D., Goswami, R.R., Grinev, D., Houston, A., Hu, Y., Liu, J., Mooney, S., Pajor, R., Sleutel, S., Tarquis, A., Wang, W., Wei, Q., Sezgin, M., 2010. Observer-dependent variability of the thresholding step in the quantitative analysis of soil images and X-ray microtomography data. Geoderma 157 (1–2), 51–63.

Bronick, C.J., Lal, R., 2005. Soil structure and management: a review. Geoderma 124, 3–22.

Donnelly, E., Mothe, F., 2008. Polar Transformer. Available from http://rsbweb.nih.gov/ij/plugins/polar-transformer.html (verified 26 Jan. 2012).

Drees, L., Karathanasis, A., Wilding, L., Blevins, R., 1994. Micromorphological characteristics of long-term no-till and conventionally tilled soils. Soil Science Society of America Journal 58, 508–517.

Feeney, D., Crawford, J., Daniell, T., Hallett, P., Nunan, N., Ritz, K., Rivers, M., Young, I., 2006. Three-dimensional microorganization of the soil–root–microbe system. Microbial Ecology 52, 151–158.

Haynes, R.J., Naidu, R., 1998. Influence of lime, fertilizer and manure applications on soil organic matter content and soil physical conditions: a review. Nutrient Cycling in Agroecosystems 51, 123–137.

Hou, H., Liu, X., Liu, G., Zz, L., Liu, Y., Hhuang, Y., Ji, J., Shao, C., Wang, F., 2011. Effect of long-term located organic–inorganic fertilizer application on rice yield and soil fertility in red soil area of China. Scientia Agricultura Sinica 44, 516–523.

Huang, S., Peng, X., Huang, Q., Zhang, W., 2010. Soil aggregation and organic carbon fractions affected by long-term fertilization in a red soil of subtropical China. Geoderma 154, 364–369.

Iassonov, P., Gebrenegus, T., Tuller, M., 2009. Segmentation of X-ray computed tomography images of porous materials: a crucial step for characterization and quantitative analysis of pore structures. Water Resources Research 45, W09415. http://dx.doi.org/10.1029/2009WR008087.

Jassogne, L., McNeill, A., Chittleborough, D., 2007. 3D-visualization and analysis of macro- and meso-porosity of the upper horizons of a sodic, texture-contrast soil. European Journal of Soil Science 58, 589–598.

Kravchenko, A., Smucker, A., AJM Rivers, M., 2011. Long-term differences in tillage and land use affect intra-aggregate pore heterogeneity. Soil Science Society of America Journal 75 (5), 1658–1666.

Lai, Q., Li, C., Huang, Q., 1992. Effect of continuous application of inorganic fertilizer on soil structure properties of paddy soil derived from red soil. (In Chinese with English abstract.) Acta Pedologica Sinica 29, 168–174.

Le Bissonnais, Y., 1996. Aggregate stability and assessment of soil crustability and erodibility: I. Theory and methodology. European Journal of Soil Science 47, 425–437.

Lee, T.C., Kashyap, R., Chu, C.N., 1994. Building skeleton models via 3-D medial surface/axis thinning algorithms. Graphical Models and Image Processing 56, 462–478.

Lindquist, W.B., Venkatarangan, A., 1999. Investigating 3D geometry of porous media from high resolution images. Physics and Chemistry of the Earth, Parts A 24, 593–599.

Lindquist, W.B., Venkatarangan, A., Dunsmuir, J., Wong, T., 2000. Pore and throat size distribution measured from synchrotron X-ray tomographic images of Fontainebleau sandstones. Journal of Geophysical Research 105B, 21508–21528.

Luo, L., Lin, H., 2009. Lacunarity and fractal analyses of soil macropores and preferential transport using micro-X-ray computed tomography. Vadose Zone Journal 8, 233.

Luo, L., Lin, H., Halleck, P., 2008. Quantifying soil structure and preferential flow in intact soil using X-ray computed tomography. Soil Science Society of America Journal 72, 1058–1069.

Luo, L., Lin, H., Li, S., 2010. Quantification of 3-d soil macropore networks in different soil types and land uses using computed tomography. Journal of Hydrology 393, 53–64.

Oades, J., 1984. Soil organic matter and structural stability: mechanisms and implications for management. Plant and Soil 76, 319–337.

Oades, J., Waters, A., 1991. Aggregate hierarchy in soils. Australian Journal of Soil Research 29, 815–828.

Oh, W., Lindquist, W.B., 1999. Image thresholding by indicator kriging. IEEE Transactions on Pattern Analysis and Machine Intelligence 21, 1–13.

Pagliai, M., LaMarca, M., Lucamante, G., 1983. Micromorphometric and micromorphological investigations of a clay loam soil in viticulture under zero and conventional tillage. European Journal of Soil Science 34, 391–403.

Pagliai, M., La Marca, M., Lucamante, G., Genovese, L., 1984. Effects of zero and conventional tillage on the length and irregularity of elongated pores in a clay loam soil under viticulture. Soil and Tillage Research 4, 433–444.

Pagliai, M., Vignozzi, N., Pellegrini, S., 2004. Soil structure and the effect of management practices. Soil and Tillage Research 79, 131–143.

Perret, J., Prasher, S., Kantzas, A., Langford, C., 1999. Three-dimensional quantification of macropore networks in undisturbed soil cores. Soil Science Society of America Journal 63, 1530–1543.

Peth, S., Horn, R., Beckmann, F., Donath, T., Fischer, J., Smucker, A., 2008. Three-dimensional quantification of intra-aggregate pore–space features using synchrotron-radiation-based microtomography. Soil Science Society of America Journal 72, 897.

Rasband, W.S., 2010. ImageJ: Image Processing and Analysis in Java. Available from the U.S. National Institutes of Health, Bethesda, Maryland, SA http://rsb.info.nih.gov/ij/ (verified 14 Oct. 2010).

Sainju, U., Whitehead, W., Singh, B., 2003. Cover crops and nitrogen fertilization effects on soil aggregation and carbon and nitrogen pools. Canadian Journal of Soil Science 83, 155–165.

SAS Institute, 1990. SAS Procedures Guide. Version 6, 3rd ed. SAS Inst, Cary, NC.

Schlüter, S., Weller, U., Vogel, H.-J., 2010. Segmentation of X-ray microtomography images of soil using gradient masks. Computers & Geosciences 10, 1246–1251.

Schlüter, S., Weller, U., Vogel, H.-J., 2011. Soil structure development including seasonal dynamics in a long-term fertilization experiment. Journal of Plant Nutrition and Soil Science 174 (3), 395–403.

Six, J., Elliott, E.T., Paustian, K., Doran, J.W., 1998. Aggregation and soil organic matter accumulation in cultivated and native grassland soils. Soil Science Society of America Journal 62, 1367–1377.

Six, J., Bossuyt, H., Degryze, S., Denef, K., 2004. A history of research on the link between (micro) aggregates, soil biota, and soil organic matter dynamics. Soil and Tillage Research 79, 7–31.

Soil Survey Laboratory Methods Manual, 2004. http://soils.usda.gov/technical/lmm.

Tisdall, J.M., Oades, J.M., 1982. Organic matter and water-stable aggregates in soils. Journal of Soil Science 33, 141–163.

Udawatta, R., Anderson, S., Gantzer, C., Garrett, H., 2006. Agroforestry and grass buffer influence on macropore characteristics: a computed tomography analysis. Soil Science Society of America Journal 70, 1763–1773.

Udawatta, R., Anderson, S., Gantzer, C., Garrett, H., 2008a. Influence of prairie restoration on CT-measured soil pore characteristics. Journal of Environmental Quality 37, 219–228.

Udawatta, R., Gantzer, C., Anderson, S., Garrett, H., 2008b. Agroforestry and grass buffer effects on pore characteristics measured by high-resolution X-ray computed tomography. Soil Science Society of America Journal 72, 295–304.

VandenBygaart, A., Protz, R., Tomlin, A., Miller, J., 1999. Tillage system effects on near-surface soil morphology: observations from the landscape to micro-scale in silt loam soils of southwestern Ontario. Soil and Tillage Research 51, 139–149.

Vogel, H., 1997. Morphological determination of pore connectivity as a function of pore size using serial sections. European Journal of Soil Science 48, 365–377.

Vogel, H., Weller, U., Babel, U., 1993. Estimating orientation and width of channels and cracks at soil polished blocks — a stereological approach. Geoderma 56, 301–316.

Wang, M.C., Yang, C.H., 2003. Type of fertilizer applied to a paddy–upland rotation affects selected soil quality attributes. Geoderma 114 (1–2), 93–108.

Wang, B.R., Cai, Z.J., Li, D.C., 2010. Effect of different long-term fertilization on the fertility of red upland soil. (In Chinese with English abstract.) Journal of Soil and Water Conservation 24, 85–88.

Wang, W., Kravchenko, A.N., Smucker, A.J.M., Rivers, M.L., 2011. Comparison of image segmentation methods in simulated 2D and 3D microtomographic images of soil aggregates. Geoderma 162, 231–241.
Whalen, J.K., Chang, C., 2002. Macroaggregate characteristics in cultivated soils after 25 annual manure applications. Soil Science Society of America Journal 66, 1637–1647.
Wildenschild, D., Vaz, C., Rivers, M., Rikard, D., Christensen, B., 2002. Using X-ray computed tomography in hydrology: systems, resolutions, and limitations. Journal of Hydrology 267, 285–297.
Young, I., Crawford, J., Rappoldt, C., 2001. New methods and models for characterising structural heterogeneity of soil. Soil and Tillage Research 61, 33–45.
Zhang, B., Horn, R., 2001. Mechanisms of aggregate stabilization in Ultisols from subtropical China. Geoderma 99, 123–145.
Zhang, B., Peng, X.H., 2006. Soil organic matter enrichment and aggregate stabilization in a severely degraded Ultisol after reforestation. Pedosphere 16, 699–706.
Zhang, H.M., Wang, B.R., Xu, M.G., Fan, T.L., 2009. Crop yield and soil responses to long-term fertilization on a red soil in southern China. Pedosphere 19 (2), 199–207.